A dual-polarized and reconfigurable reflectarray for generation of vortex radio waves

Cite as: AIP Advances **8**, 055331 (2018); https://doi.org/10.1063/1.5023282
Submitted: 23 January 2018 • Accepted: 21 May 2018 • Published Online: 30 May 2018

Chen-Chen Li, Lin-Sheng Wu and Wen-Yan Yin

A dual-polarized and reconfigurable reflectarray for generation of vortex radio waves

Chen-Chen Li,[1] Lin-Sheng Wu,[2,a] and Wen-Yan Yin[1,b]
[1]*Innovative Institute of Electromagnetic Information and Electronic Integration, Zhejiang Provincial Key Lab of Advanced Micro-Nano Electronic Devices and Smart Systems, Zhejiang University, Hangzhou 310058, China*
[2]*Key Laboratory of Ministry of Education of Design and Electromagnetic Compatibility of High-Speed Electronic Systems, Shanghai Jiao Tong University, Shanghai 200240, China*

(Received 23 January 2018; accepted 21 May 2018; published online 30 May 2018)

Electromagnetic (EM) waves with orbital angular momentum (OAM) provide a new degree of freedom for channel multiplexing to improve the capacity of wireless communication. For OAM-based systems, it is important to design specific configurations to generate vortex radios. In this paper, a reconfigurable reflectarray antenna is proposed with independent control of dual polarizations. A reflective cell is proposed by properly assigning the variable capacitances of four varactors, which are placed between metal square rings of each unit. The varactors of each unit are divided into two groups and the capacitance value of each group controls the reflection phase for a single linear polarization. By using the equivalent circuit model, the reflective units and array can be designed efficiently. Smooth phase variation and good reflection efficiency are achieved. Then, the reflectarray is set into sectors and a simple phase-shifting surface model is used to generate vortex beam. Each sector is realized with reflective units satisfying desired reflection phases for different modes. This kind of OAM-generating method can reduce the required variation range of reflection phase and provide more choices for a specific OAM mode combination with dual polarization, which is helpful to reduce mutual coupling between the two linear polarizations. Finally, full-wave simulations show that the 0, ±1, ±2 modes of vortex beam are successfully generated at 3.5 GHz with arbitrary combination in dual-polarization, which is also supported by OAM modes purity and reflection efficiency analysis. Therefore, in our design, the reconfigurable OAM and spin angular momentum (SAM), related with polarization, can be utilized simultaneously and independently for high-capacity wireless communication. https://doi.org/10.1063/1.5023282

I. INTRODUCTION

Vortex waves carrying orbital angular momentum (OAM) have infinite orthogonal states in theory, while electromagnetic wave with spin angular momentum (SAM) has only two orthogonal states. Therefore, OAM has attractive potential to significantly increase spectral efficiency and channel capacity for wireless communication.[1]

Early studies focus on OAM-carrying beams in optical region,[2,3] but recently, many studies indicate that OAM can also be applied to radio frequencies. In 2007, Thide et al. demonstrated that vortex radio beams can be generated by vector antenna arrays in low-frequency radio domain, which was validated by simulations.[4] In 2012, Tamburini et al. carried out date transmitting via vortex waves in radio frequency experimentally by using Yagi–Uda and helicoidal parabolic antennas.[5]

[a]E-mail: wallish@sjtu.edu.cn
[b]E-mail: wyyin@zju.edu.cn

Tennant and Allen demonstrated that multiple OAM modes could be produced by using time-switched arrays.[6] Gradually, studies on OAM-carrying beams for radio communication have become a hotspot. Although it may be argued that OAM is only a subset of multiple-in-multiple-out (MIMO) communication systems,[7] OAM has the potential to compliment the performance of the MIMO system, such as low receiver computational complexity.[8] Within an OAM radio system, it is essential to explore functional antennas to generate vortex beams. In 2014, L. Cheng et al. demonstrated experimentally a spiral phase plate (SPP) to generate arbitrary mixed OAM beams around 94 GHz.[9] In 2016, L. Li et al. proposed three reflective metasurfaces for the generation of different modes and polarizations of vortex radio waves in diverse directions at 5.8 GHz.[10–12] In 2017, a traveling-wave circular slot antenna was proposed for the generation and multiplexing of OAM waves at 10 GHz.[13] A reconfigurable graphene reflectarray antenna was proposed to generate vortex beams in THz band.[14] However, vortex-wave-generating antennas still remain unreconfigurable in the radio frequency till now.

Recent studies show many reconfigurable reflectarrays using varactors, MEMS switches, PIN diodes and Liquid Crystal,[15–19] which are mainly aimed at beam scanning and antenna models changing. Varactor based reflectarrays have the potential of achieving OAM modes tuning because it can be tuned continuously. Different from the work in Ref. 20, where varactor diode-tuned elements were used to achieve an electronically tunable reflectarray,[20] the element proposed in this work can be controlled in dual-polarization with little mutual coupling effect.

In this article, we propose a reflectarray with units, constructed with metal square rings and electrically tunable varactors. Different from the work in Ref. 11, where a dual polarized metasurface able to generate one fixed OAM state was designed, our proposed reflectarray can generate 25 combinations of OAM modes reconfigurably by changing capacitance values of varactors, keeping dual polarization original characteristics. In Section II, the geometries of unit and reflectarray are given and modelled, and the mechanism of vortex generation is explained. In Section III, numerical investigations are further carried out to show that dual-polarized vortex waves with different OAM modes can be produced with the proposed reflectarray antenna in radio frequency. Finally, a conclusion is drawn in Section IV.

II. GEOMETRIES OF UNIT AND REFLECTARRAY

A. Description of unit structure

As shown in Fig. 1(a), four metal patches with square hollows inside, which make them square rings, and gaps between them, where in the middle a varactor diode is placed, are selected as the unit cell of the proposed reflectarray. The length of square hollows and gap are 2.5 and 1.8 mm, respectively.

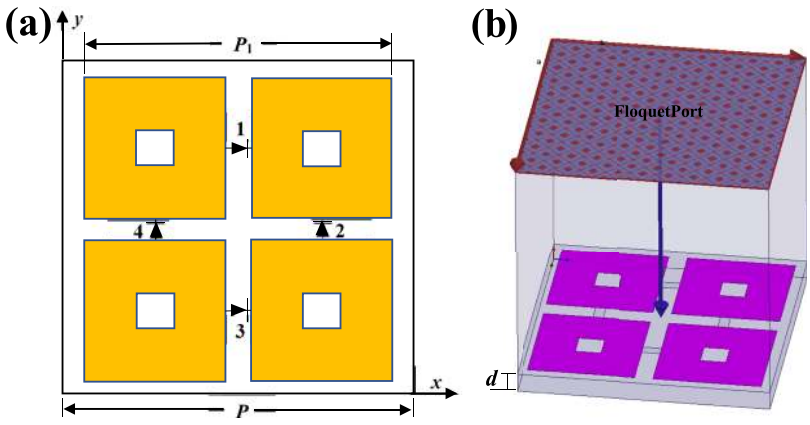

FIG. 1. (a) Unit structure of reflectarray and (b) unit model simulated in HFSS. This unit cell is composed of four metal square rings with varactor diodes between them. The period of reflective cell is P=25 mm. The permittivity and thickness of the dielectric substrate are set to ε_r=2.65, d=1.9 mm.

The varactor diodes numbered 1 and 3 are with the capacitance of C_1, while those numbered 2 and 4 are with the capacitance of D_1. Each element consists of a back-grounded substrate (ε_r=2.65) with the thickness of 1.9 mm and four metal square rings printed on the top plane, where the length P_1 is set to 23 mm. The period of reflective cell is P=25 mm.

With the tuning of biasing voltages between adjacent rings, the capacitances of varactor diodes in each unit can be controlled to get a desired reflection phase. It is easy to understand that four biasing voltages of 0, V_1, V_2 and V_1+V_2 should be properly assigned for patches, where V_1 and V_2 are used to control C_1 and D_1, respectively. An infinite periodic model, full-wave simulated with ANSYS HFSS, is used to analyze the reflection phase characteristic of unit, as shown in Fig. 1(b).

B. Equivalent circuit model

To better understand the principle of proposed structure and speed up the design procedure, a simple equivalent circuit model is used. As shown in Fig. 2(a), with plane wave of y-polarization, metal square patches are modeled as inductors with the lower and upper two rings as a unit block. Due to the symmetry of this structure, the two inductors have the same value L_1, as shown in Figure 2. The varactor-loaded horizontal gap acts as a capacitance C, which is shown in Fig. 2(a). The capacitive gap contributes to a constant capacitance of C_f while the varactor diodes over the gap provide a tunable capacitance of D_1, as shown in Fig. 2(b).[21] The substrate of a unit is equal to a transmission line TL in Fig. 2(b) with characteristic impedance of Z and electrical length of L, which are calculated by Equations (1) and (2), respectively. The reference frequency for electrical length is 3.5 GHz.

$$Z = \frac{Z_0}{\sqrt{\varepsilon_r}} \tag{1}$$

$$L = \frac{360^\circ}{\lambda} d \tag{2}$$

where Z_0 is the intrinsic impedance in free space, ε_r is relative permittivity of substrate, d is the thickness of substrate, λ is wavelength in substrate.

To obtain the value of L_1 and C_f, we simulate the unit structure first in HFSS with constant value of D_1. When we obtain reflection phase curve with frequency ranging from 2.5 GHz and 4.5 GHz, we introduce it to Advanced Design System (ADS) to make a fitting between the full-wave model in HFSS and the equivalent circuit model. As shown in Figure 3, good agreement has been achieved when the value of D_1 is then changed.

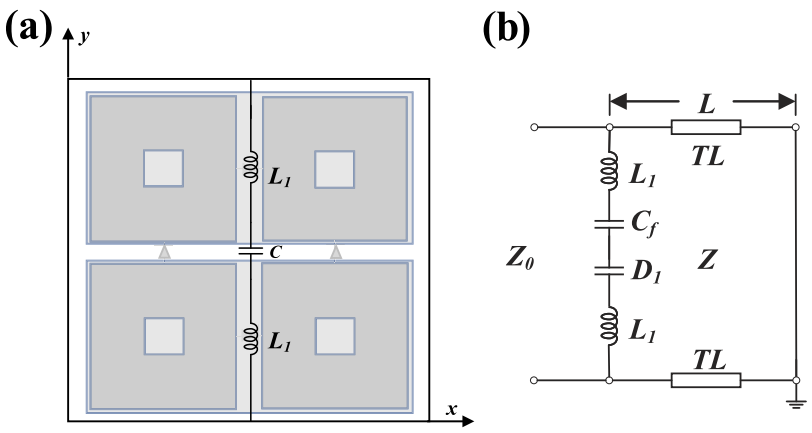

FIG. 2. (a) Simple model of reflectarray unit cell and (b) The equivalent circuit model of a unit. Characteristic impedance of free space is Z_0=377 Ω. C=C_f+D_1 where C_f and D_1 are constant part and variable part of total capacitance C, respectively. L_1 is the inductance of metal patches. Z and L are characteristic impedance and electrical length of transmission line TL, respectively.

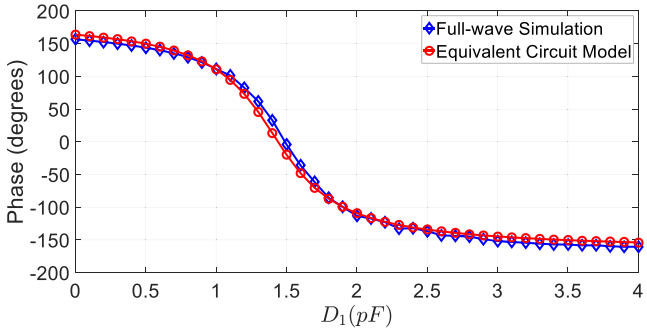

FIG. 3. Reflection phase obtained by full-wave simulation and equivalent circuit model.

C. Reflectarray antenna

A reflective surface model consisting of N sectors is used to generate vortex radio waves, as shown in Fig. 4.[14] It is excited by a normally incident plane wave and phase variation increment over one circle is an integer multiple l of 2π. Assuming that the excitation is an x-polarized TEM wave propagating along -z direction, it can be simply defined as

$$E_x = E_0 \exp(-ikz) \tag{3}$$

Without consideration of boundary matching, the primitive reflected field for each sector at z=0 can be expressed as[22]

$$E_{nx}|_{z=0} = E_R \exp\left(i\frac{2l\pi}{N}n\right), (n = 0, 1, ..., N-1) \tag{4}$$

where n is the serial number of the sectors, l is the topological charge of OAM to be generated. The far-field expression of reflected field can be expressed as[22]

$$E_\theta = \frac{Ake^{ikr}e^{il\varphi}}{ir}\cos\varphi \sin^l\theta[{}_1F_2(\theta)] \tag{5}$$

$$E_\varphi = \frac{Ake^{ikr}e^{il\varphi}}{-ir}\sin\varphi\cos\theta \sin^l\theta[{}_1F_2(\theta)] \tag{6}$$

where ${}_1F_2(\theta)$ is a hypergeometric function, A is a constant related to l and k.

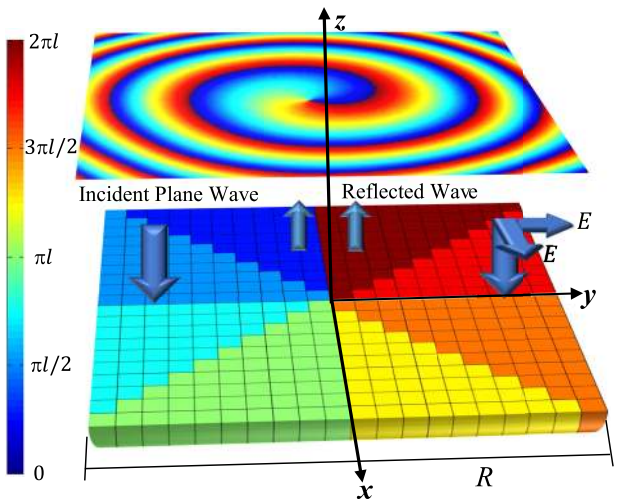

FIG. 4. Reflective surface model consisting of N sectors with varying phase from 0 to 2lπ, which is excited by a plane wave.

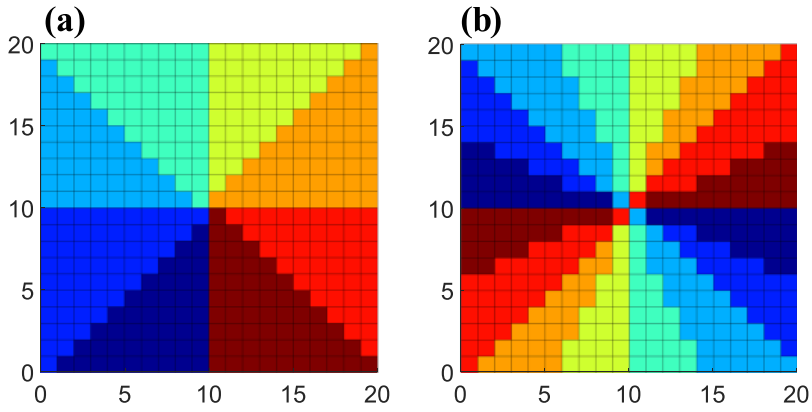

FIG. 5. (a) 8 sectors for the generation of OAM modes ±1 and (b) 16 sectors for the generation of OAM modes ±2.

All the components of E-fields generated by this plane have the same phase factor $\exp(il\varphi)$. In our design, the reflectarray antenna, with 20×20 units, occupies a square area of 50×50 cm^2. As shown in Fig. 5(a), in order to generate the OAM ±1 mode, the reflectarray is divided into 8 sectors with 45° reflection phase difference between two adjacent sectors. To maintain the phase difference above when the OAM mode is turned to l=±2, the reflectarray is divided into 16 sectors, as shown in Fig. 5(b).

III. NUMERICAL RESULTS AND DISCUSSION

A. Reflection phase versus capacitances

As obtained with HFSS, the reflection phase is a function of capacitance under normal incidence. With the control of C_1 and D_1 respectively, the unit shows a continuous reflection phase behavior within a range over 300° on both x- and y-polarized waves. Fig. 6 shows the magnitude and phase of reflected E-field versus the value of capacitance D_1 in the y-polarization at 3.5 GHz. With different values of D_1, the reflection amplitudes coefficients remain 1. As depicted in Fig. 6(b), The capacitance C_1 in the x-polarization has a little impact on the reflection characteristic. Due to the symmetry of unit structure, the reflection phase characteristic versus the capacitance C_1 of x-polarization is almost the same as that shown in Fig. 6(b). To reduce errors when different modes of vortex waves are produced for different polarizations simultaneously, we further sweep the values of C_1 and D_1 from 0 to 4 pF, which are not shown here, and average all these curves to get a smooth one, as plotted in Fig. 6(b). A tunable phase within the range of 317° is achieved. Generally, to realize OAM-carrying beams, a full range from -180° to 180° should be applied. Thanks to the OAM-generating model in Figure 4, the reflectarray is divided into sectors and the reflection phases can be set discretely. Desired reflection phases can be satisfied with the parameters listed in Table I.

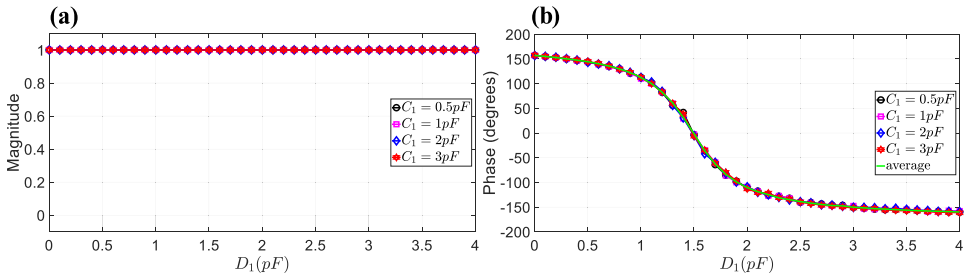

FIG. 6. Simulated reflection (a) Magnitude and (b) Phase as the function of capacitance.

TABLE I. Capacitance values of each sector (Unit: pF).

Sector \ Mode	0	-1	1	-2	2
0	2	3.9407	0.1507	3.9407	0.1507
1	2	2.1408	1.1103	2.1408	1.1103
2	2	1.8291	1.3764	1.8291	1.3764
3	2	1.6655	1.5307	1.6655	1.5307
4	2	1.5307	1.6655	1.5307	1.6655
5	2	1.3764	1.8291	1.3764	1.8291
6	2	1.1103	2.1408	1.1103	2.1408
7	2	0.1507	3.9407	0.1507	3.9407

In our simulations, the reflectarray is divided into 16 sectors to generate the OAM-carrying beam of modes ±2, as shown in Fig. 5(b). Only the first 8 capacitance values are listed in Table I and they will be repeated for the last 8 capacitance values.

B. Far-field phase distribution

Figure 4 shows the reconfigurable reflectarray corresponding to OAM modes l=1, where different colors correspond to different values of capacitance. In order to generate a dual-polarized reconfigurable OAM-carrying wave by a single reflectarray antenna, it is excited with either x- or y-polarized E-field plane waves and the sectored reflective surface is utilized with properly assigned reflection phases. Under this condition, the OAM with a mode l can be generated in both x- and y-polarizations if the phase shift between sectors is $2\pi l/N$ corresponding to both C_1 and D_1, respectively. The topological charge l and the sector number N should meet the relation of $-N/2 < l < -N/2$. To get good magnitude patterns for higher-order OAM modes, more sectors are desired. For the OAM mode l=±2, the phase difference of ±45° between adjacent sectors is selected, leading to 16 sectors. Furthermore, if C_1 and D_1 are tuned independently, the combination of different OAM modes in dual polarizations can be generated simultaneously, such as the OAM mode of l=1 and of l=-1 in y-polarization and x-polarization respectively, or both the OAM mode of l=2 in x- and y-polarizations. There are 20×20 reflective units utilized to build up the reflectarray, resulting in the side length of 500 mm (about 5.8 wavelengths in free space). The values of capacitance of each sector are changed to reconfigure the reflectarray, while the patch size of each unit remains the same.

The observation plane of far-field phase distributions is at 8 m (about 93 wavelengths in free space) above the reflectarray and is normal to the z-axis. According to our simulations, phase distributions are almost the same when observed at different heights. Figure 7 shows the simulated phase patterns of different OAM mode combinations in dual-polarization at 3.5 GHz. The change from blue to red colors corresponds to the phase variation of 360°. It is clearly seen that the twisted phase patterns of OAM-carrying beams with the modes of l=0, l=±1 and l=±2 are realized successfully. Limited by the size of reflectarray, the phase distribution of OAM wave with the mode of l=0 shows distortion near the edges, but good performance is observed in the middle region. Furthermore, as shown in Figure 7, various OAM mode combinations are successfully generated in dual polarizations and controlled independently.

Figure 8 shows the simulated magnitude patterns of selected OAM mode combinations, corresponding to Fig. 7(b) and 7(c). It is clearly seen that typical doughnut-like E-field magnitude patterns are obtained for higher-order OAM modes, although the field patterns degrade slightly in our simulations due to the mutual coupling effects between two polarizations. Thanks to the independent controlling of C_1 and D_1, there are many combinations of C_1 and D_1 for a specific OAM mode combination. For example, for the mode combination of l=1 and l=-1 in y- and x-polarizations respectively, 8 sectors are used. Maintaining the capacitance values of C_1 for the units in these sectors, the capacitances D_1 can still vary when the phase difference between adjacent sectors is guaranteed to be equal to 45°. So, there are 8 choices available to this mode combination. One can choose the best values of capacitance in consideration of both magnitude and phase patterns.

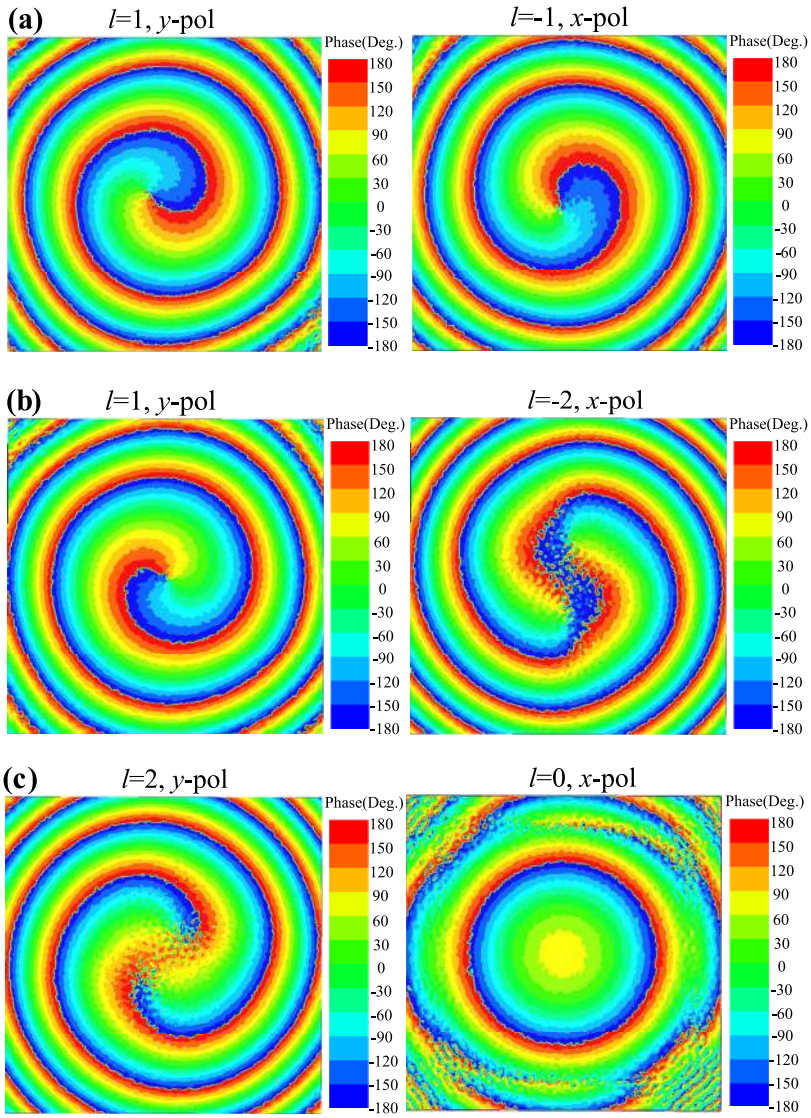

FIG. 7. Simultaneously and independently generated phase patterns of the vortex radio waves with different modes and polarizations: (a) l=1 for y-pol and l=-1 for x-pol; (b) l=1 for y-pol and l=-2 for x-pol and (c) l=2 for y-pol and l=0 for x-pol.

Figure 9 demonstrates phase patterns of different OAM modes along azimuthal coordinate at a constant radius of 700 mm. The observation plane is placed at the same height of Figure 7. Figure 9 shows the desired linear dependence between the spatial phase and azimuthal angle with a little distortion.[23] The gradients of the lines corresponding to OAM mode 1, -1, 2, -2 are 0.99, -1, 1.94, -1.96, respectively. Similar results can be obtained for different combinations of OAM modes in dual-polarization according to our simulations.

Next, we do efficiency analysis for our proposed reflectarray antenna of OAM modes l=1 for y-polarization and l=-1 for x-polarization. Reflection efficiency is almost the same for different OAM modes combinations according to our simulations. The EM energy can be calculated by[24]

$$U = \oint_A \mathbf{S} \cdot d\mathbf{A} \tag{7}$$

where A is a closed surface and $\mathbf{S}$ is the Poynting vector.

We choose A as a rectangular box containing this reflectarray antenna and the gap between them is 10 mm. If we consider efficiency as the ratio of reflection energy to the total energy of incidence

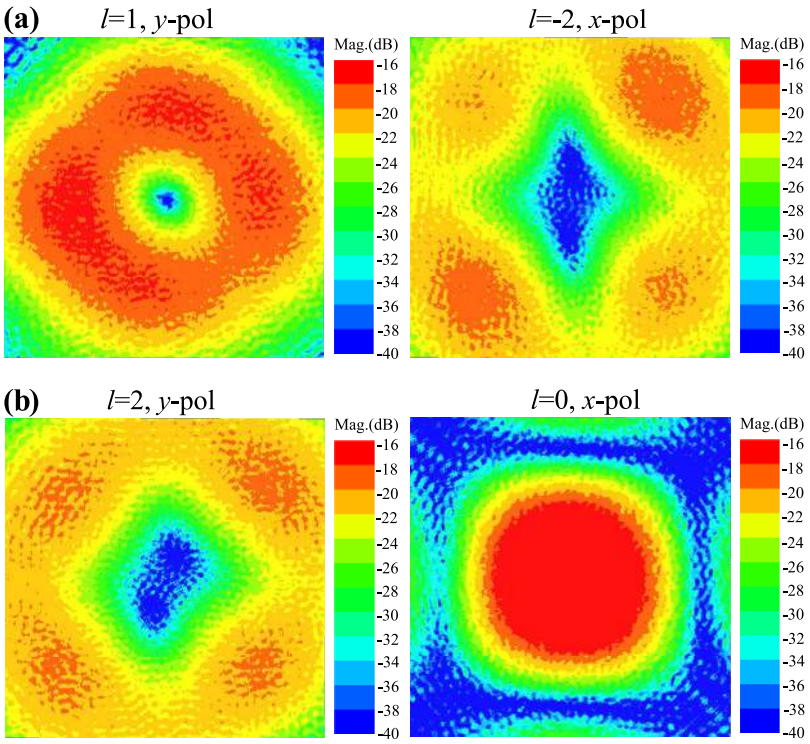

FIG. 8. Corresponding magnitude patterns to Figure 6 with different modes and polarizations: (a) l=1 for y-pol and l=-2 for x-pol, corresponding to Fig. 7(b) and (b) l=2 for y-pol and l=0 for x-pol, corresponding to Fig. 7(c).

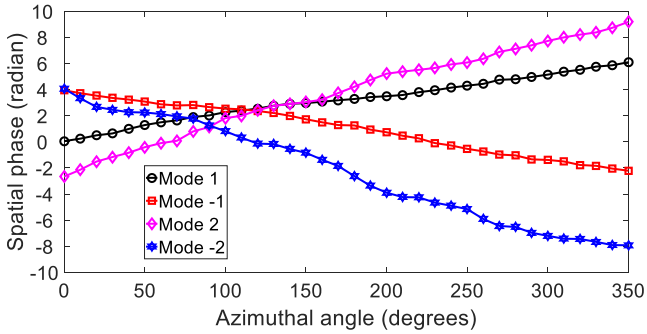

FIG. 9. Phase patterns of different OAM modes along the azimuthal coordinate at a constant radius of 700 mm.

wave which is calculated as the sum of the energy of reflected and transmitted wave, the efficiency is nearly 100% (96.77%).

IV. CONCLUSION

In conclusion, we propose a reflectarray antenna to produce reconfigurable OAM-carrying waves for dual polarizations independently in radio frequency. The reflectarray is sectored and assigned with specific reflection phases. Each sector is constructed by units with four metal square rings mounted with four varactor diodes. As demonstrated numerically, the reflection phases can be controlled by tuning capacitances independently for x- and y-polarizations. When excited by a plane wave, the reflectarray could be independently reconfigured in dual-polarization with different values of capacitance in each sector for the generation of the 0, ±1 and ±2 modes of vortex radio waves.

The proposed reconfigurable reflectarray is promising for future applications in radio frequency communication systems.

ACKNOWLEDGMENTS

This work was supported by the National Natural Science Foundation of China under Grants 61431014 and 61622113.

[1] J. Wang *et al.*, Nat. Photon. **6**, 488 (2012).
[2] L. Allen, M. W. Beijersbergen, R. J. C. Spreeuw, and J. P. Woerdman, Phys. Rev. A **45**, 8185 (1992).
[3] M. W. Beijersbergen, R. P. C. Coerwinkel, M. Kristensen, and J. P. Woerdman, Opt. Commun. **112**, 321 (1994).
[4] B. Thide *et al.*, Phys. Rev. Lett. **99**, 087701 (2007).
[5] F. Tamburini, E. Mari, A. Sponselli, B. Thide, A. Bianchini, and F. Romanato, New J. Phys. **14**, 811 (2012).
[6] A. Tennant and B. Allen, Electron. Lett. **48**, 1365 (2012).
[7] O. Edfors and A. J. Johansson, IEEE Trans. Antennas Propag. **60**, 1126 (2012).
[8] W. Zhang *et al.*, IEEE Trans. Wireless Commun. **16**, 1308 (2017).
[9] L. Cheng, W. Hong, and Z. C. Hao, Sci. Rep. **4**, 4814 (2014).
[10] S. X. Yu, L. Li, G. M. Shi, C. Zhu, X. X. Zhou, and Y. Shi, Appl. Phys. Lett. **108**, 5448 (2016).
[11] S. X. Yu, L. Li, and G. M. Shi, Appl. Phys. Express **9**, 082202 (2016).
[12] S. X. Yu, L. Li, G. M. Shi, C. Zhu, and Y. Shi, Appl. Phys. Lett. **108**, 662 (2016).
[13] Z. F. Zhang, S. L. Zheng, X. F. Jin, H. Chi, and X. M. Zhang, IEEE Antennas Wireless Propag. Lett. **16**, 8 (2017).
[14] Z. Chang, B. You, L.-S. Wu, M. Tang, Y.-P. Zhang, and J.-F. Mao, IEEE Antennas Wireless Propag. Lett. **15**, 1537 (2016).
[15] S. V. Hum and J. Perruisseau-Carrier, IEEE Trans. Antennas Propag. **62**, 183 (2014).
[16] F. Venneri, S. Costanzo, and G. Di Massa, IEEE Trans. Antennas Propag. **61**, 635 (2013).
[17] T. Debogovic and J. Perruisseau-Carrier, IEEE Trans. Antennas Propag. **62**, 5055 (2014).
[18] H. H. Yang *et al.*, IEEE Trans. Antennas Propag. **64**, 2246 (2016).
[19] S. Bildik, S. Dieter, C. Fritzsch, W. Menzel, and R. Jakoby, IEEE Trans. Antennas Propag. **63**, 122 (2015).
[20] S. V. Hum, M. Okoniewski, and R. J. Davies, IEEE Microw. Wireless Compon. Lett. **15**, 422 (2005).
[21] F. Costa and A. Monorchio, IEEE Trans. Antennas Propag. **60**, 4650 (2012).
[22] B. You, L. Zhou, L.-S. Wu, Y.-P. Zhang, and J.-F. Mao, IEEE Trans. Antennas Propag. **64**, 4942 (2016).
[23] M. L. N. Chen, L. J. Jiang, and W. E. I. Sha, J. Appl. Phys. **119**, 033126 (2016).
[24] M. L. N. Chen, L. J. Jiang, and W. E. I. Sha, IEEE Trans. Antennas Propag. **65**, 396 (2017).